Model Predictive Control of Battery-Powered Trains for Catenary-Free Operation ⋆

Alessio La Bella * **Gian Paolo Incremona** *
Aline Cristiane Buzzi ** **Patrizio Colaneri** *

* *Dipartimento di Elettronica, Informazione e Bioingegneria, Politecnico di Milano, Piazza Leonardo da Vinci 32, 20133 Milan, Italy (e-mail:{alessio.labella, gianpaolo.incremona, patrizio.colaneri}@polimi.it)*
** *Alstom SESTO, Via Fosse Ardeatine, 120, 20099 Sesto San Giovanni, Milan, Italy (e-mail: aline-cristiane.buzzi@alstomgroup.com)*

Abstract: Rail transportation is recently making a comeback with stunning results from technological viewpoint. While the efficiency of trains is well known, many aspects related to energy management still need to be tackled, including sustainability and optimization issues. These issues are central to the control community, and in this context model predictive control (MPC) is a powerful control approach for its capability of guaranteeing constraints satisfaction, while minimizing a predefined cost function. In this article, we exploit these advantages to provide more efficient control of the electric equipment inside railway vehicles. More precisely, the proposed MPC approach is capable of addressing the challenging scenario of partially catenary-free tracks for trains. These are equipped with batteries, which have to supply traction motors and parallel-connected auxiliary loads in an efficient manner, while reducing the amount of losses over the electric lines. Simulation results, based on real data provided by the industrial partner Alstom rail transport, show the effectiveness of the proposal.

Keywords: Model predictive control, power converters, railway vehicles.

1. INTRODUCTION

Nowadays, because of its reduced energy consumption, rail is already the greenest and strategic transportation sector in the transition process towards moving forms powered by green, low-carbon energy. In fact, in the last decades, different sustainable solutions have been proposed to further improve the train energy consumption, through both vehicles technology upgrades, and control-based techniques (Scheepmaker et al., 2017).

Among these control-based works, for instance, eco-drive control is a valid solution to the problem of generating optimal driving sequences taking into account a trade-off between energy consumption and travel time, see e.g., (Farooqi, 2019). Such a method has been also exploited to recover braking energy which otherwise would be lost in the train rheostats. Specifically, collaborative eco-drive control approaches have been proposed, for instance as in (Farooqi et al., 2019), where a network of trains, modelled as Markov systems interacting among each other, are induced to use the energy deriving from braking of other trains in order to accelerate, thus avoiding energy supply from the main grid. Most of these works are based on optimization methods (see e.g., (Howlett, 2000)), relying on a switched characterization of the train dynamics whose motion is captured by four operation modes, i.e., acceleration, cruising, coasting and braking (Albrecht et al., 2016).

Another important aspect for train energy efficiency is the power control to supply auxiliary services (e.g., heating, cooling or lightning). Classical solutions relied on centralized architectures, which were not very efficient in the low power range, and adopted expensive and bulky voltage source converters (VSCs). Recently, as an alternative, parallel-connected converters are an efficient solution to power distribution in railway vehicles in order to minimize the current circulating among auxiliary services, and possibly traction motors, hence achieving load sharing and losses reduction. Droop-control based solutions are the most adopted methodologies in this framework, where virtual impedance control (Kim et al., 2011), or voltage-current droop control (Li et al., 2018) have been proposed, among many other techniques. Also robust approaches, such as sliding mode control methods based on a droop-like sliding variable (Buzzi et al., 2020), have been introduced.

Moreover, these works often assume the presence of the catenary grid over all the train track, so as to ensure a power source to the trains, both for traction and auxil-

⋆ This is the final version of the accepted paper submitted for inclusion in the Proceedings of the 22nd IFAC World Congress 2023, Yokohama, Japan, July 2023, doi:10.1016/j.ifacol.2023.10.1089. This work has been partially supported by the Italian Ministry for Research in the framework of the 2017 Program for Research Projects of National Interest (PRIN), Grant no. 2017YKXYXJ.

iary services, whenever no energy exchange among them occurs. Therefore, a recent paradigm for train power distribution based on catenary-free tracks is under investigation, see e.g., (Becker and Dämmig, 2016; Al-Ezee et al., 2015). Indeed, catenary-free tracks are adopted in specific contexts, when electric lines cannot be installed due to environmental issues. However, this configuration requires the presence of on-board power sources such as batteries or fuel cells (Campillo et al., 2017; Alstom, 2016). As a consequence, the design of control techniques to manage the electric power distribution inside each train, while taking into account catenary-free tracks, becomes mandatory.

Motivated by the challenging catenary-free scenarios with additional power sources such as batteries, the main goal of this paper is to design a model predictive control (MPC) energy management system for regulating the train internal electric resources, thus maximizing its efficiency. In particular, the predictive capability of the MPC approach suits well with the time-varying catenary supply, coordinating in advance the battery charge based on the knowledge of the future track characteristics. Specifically, the proposed MPC acts as a high-level controller to provide voltage and current references tracked by suitable low-level controllers, e.g., plug-and-play regulators (Nahata et al., 2021) or sliding mode ones (Incremona et al., 2017). Moreover, the proposed MPC enables high energy savings in terms of active power losses reduction, and a proper management of the batteries state of charge, e.g., considering regenerative braking scenarios. The proposed strategy is finally applied to a realistic case study relying on data provided by Alstom rail transport.

The paper is structured as follows. In Section 2, the train electric model is described. The MPC formulation is discussed in Section 3, and the case study is presented in Section 4. Some conclusions are gathered in Section 5.

2. MODELLING AND PROBLEM STATEMENT

The electric model of the train is hereafter introduced, and the energy-management control problem is formulated.

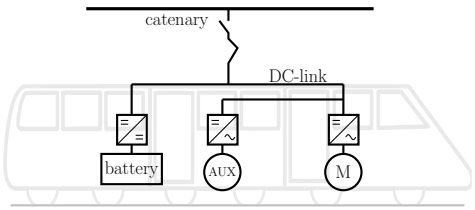

Fig. 1. Schematic representation of the train electric components.

Consider Fig. 1 where a simplified schematic rendering of the electric equipment of the train is illustrated. It includes two different energy sources, that is the catenary grid and the batteries, both connected to the DC-link. Whenever the train is disconnected from the catenary, the batteries are instrumental to supply the traction current and all the auxiliary loads, such as heating, cooling or lightning. DC/DC converters and parallel voltage source converters (VSCs) interface the DC-link with the battery internal circuit in DC, and auxiliary loads together with traction motors in alternating current (AC), respectively.

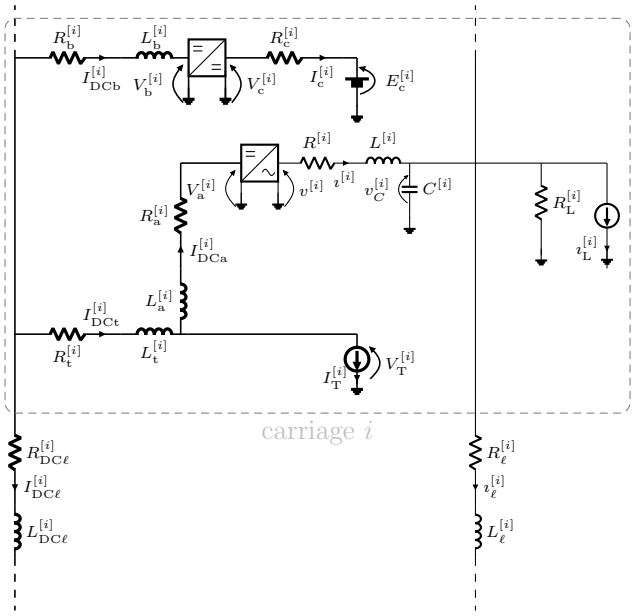

Fig. 2. Single line electric diagram for a single carriage with battery and traction motor on the DC-network (thick lines), and auxiliary load on the AC-network.

Table 1. List of symbols for the ith carriage.

Symbol	Description
$R_{\mathrm{b}}^{[i]} L_{\mathrm{b}}^{[i]}$	battery DC-network impedance
$I_{\mathrm{DCb}}^{[i]}$	battery DC-network current
$V_{\mathrm{b}}^{[i]}$	battery DC-network voltage
$R_{\mathrm{c}}^{[i]}$	battery internal resistance
$E_{\mathrm{c}}^{[i]}$	battery open circuit voltage
$I_{\mathrm{c}}^{[i]}$	battery internal current
$V_{\mathrm{c}}^{[i]}$	battery internal voltage
$R_{\mathrm{a}}^{[i]} L_{\mathrm{a}}^{[i]}$	auxiliary DC-network impedance
$I_{\mathrm{DCa}}^{[i]}$	auxiliary DC-network current
$V_{\mathrm{a}}^{[i]}$	auxiliary DC-network voltage
$R^{[i]} L^{[i]} C^{[i]}$	auxiliary AC filter
$v_C^{[i]}$	capacitor AC voltage
$i^{[i]}$	auxiliary AC-network current
$v^{[i]}$	auxiliary AC-network voltage
$R_{\mathrm{L}}^{[i]}, i_{\mathrm{L}}^{[i]}$	ZI load
$R_{\mathrm{t}}^{[i]} L_{\mathrm{t}}^{[i]}$	DC-network impedance
$I_{\mathrm{DCt}}^{[i]}$	DC-network current
$I_{\mathrm{T}}^{[i]}$	traction current
$V_{\mathrm{T}}^{[i]}$	traction voltage
$R_{\mathrm{DC}\ell}^{[i]} L_{\mathrm{DC}\ell}^{[i]}$	transit DC line impedance
$I_{\mathrm{DC}\ell}^{[i]}$	transit DC line current
$R_{\ell}^{[i]} L_{\ell}^{[i]}$	AC line impedance
$i_{\ell}^{[i]}$	AC line current

In the following we assume that the considered train has n carriages and the notation $\cdot^{[i]}$, with $i \in \mathcal{N} \coloneqq \{1, \dots, n\}$, is used to indicate variables associated to the ith carriage. Moreover, for the sake of simplicity, without any loss of generality, carriages are numbered in increasing order, meaning that the ith carriage is connected to the $(i+1)$th one for any $i \in \mathcal{N}' \coloneqq \{1, \dots, n-1\}$. Note that, in the following, the dependence of all the variables on time t will be omitted, when obvious, for the sake of compactness.

Consider now the ith carriage single line electric diagram, provided by Alstom rail transport, in Fig. 2. The definition

of all the variables is reported in Table 1. As described before, a DC/DC converter interfaces the DC-link with the battery internal circuit, as well as a VSC does the same for the AC auxiliary loads. The traction circuit is here reasonably simplified as a current generator capable of sending current towards the DC-link if braking mode occurs. All the carriages are then connected to the following and preceding ones trough both the DC-network impedances and those of the AC-network. Note that, the electric circuit could be different for each carriage, as some "buggy" carriage (i.e., without traction motors) may be present. For the sake of clarity, in order to introduce the model of the catenary grid and of the battery, the specific carriage illustrated in Fig. 2 contains all these elements, which are discussed hereafter.

2.1 DC-network

Let us use the subscripts $\cdot_{\mathrm{b}}$, $\cdot_{\mathrm{a}}$ and $\cdot_{\mathrm{t}}$ to denote all the variables associated to the battery circuit, to the auxiliary load circuit and to the transit line, which connects the auxiliary load circuit and the traction generator, respectively. Given the corresponding impedances $R_{\mathrm{b}}^{[i]}L_{\mathrm{b}}^{[i]}$, $R_{\mathrm{a}}^{[i]}L_{\mathrm{a}}^{[i]}$ and $R_{\mathrm{t}}^{[i]}L_{\mathrm{t}}^{[i]}$, one has that the DC-network equations are

$$\dot{I}_{\mathrm{DCb}}^{[i]} = \tfrac{1}{L_{\mathrm{b}}^{[i]}}\left(-R_{\mathrm{b}}^{[i]}I_{\mathrm{DCb}}^{[i]} - V_{\mathrm{b}}^{[i]} + V_{\mathrm{DC}}^{[i]}\right), \tag{1a}$$

for the battery circuit,

$$\dot{I}_{\mathrm{DCt}}^{[i]} = \tfrac{1}{L_{\mathrm{t}}^{[i]}}\left(-R_{\mathrm{t}}^{[i]}I_{\mathrm{DCt}}^{[i]} - V_{\mathrm{T}}^{[i]} + V_{\mathrm{DC}}^{[i]}\right), \tag{1b}$$

for the transit line towards the traction motor, and

$$\dot{I}_{\mathrm{DCa}}^{[i]} = \tfrac{1}{L_{\mathrm{a}}^{[i]}}\left(-R_{\mathrm{a}}^{[i]}I_{\mathrm{DCa}}^{[i]} - V_{\mathrm{a}}^{[i]} + V_{\mathrm{T}}^{[i]}\right), \tag{1c}$$

for the auxiliary load circuit, where $V_{\mathrm{DC}}^{[i]}$ is the voltage on the DC-link, while $I_{\mathrm{DCb}}^{[i]}$, $I_{\mathrm{DCa}}^{[i]}$, $I_{\mathrm{DCt}}^{[i]}$ and $V_{\mathrm{b}}^{[i]}$, $V_{\mathrm{a}}^{[i]}$, $V_{\mathrm{T}}^{[i]}$ are currents and voltages corresponding to these circuits, as described in Table 1.

Now, given the DC-link resistive-inductive line impedance between carriages i and $i+1$, namely $R_{\mathrm{DC}\ell}^{[i]}L_{\mathrm{DC}\ell}^{[i]}$, and the current flowing from carriages i and $i+1$, i.e., $I_{\mathrm{DC}\ell}^{[i]}$, with $I_{\mathrm{DC}\ell}^{[n]} = 0$, the line dynamics are captured by

$$\dot{I}_{\mathrm{DC}\ell}^{[i]} = \tfrac{1}{L_{\mathrm{DC}\ell}^{[i]}}\left(-R_{\mathrm{DC}\ell}^{[i]}I_{\mathrm{DC}\ell}^{[i]} + V_{\mathrm{DC}}^{[i]} - V_{\mathrm{DC}}^{[i+1]}\right), \tag{2a}$$

for $i \in \mathcal{N}'$. Moreover, exploiting the Kirchhoff's current law, it holds that

$$I_{\mathrm{DC}\ell}^{[i]} = I_{\mathrm{DC}\ell}^{[i-1]} - I_{\mathrm{DCb}}^{[i]} - I_{\mathrm{DCa}}^{[i]} - I_{\mathrm{T}}^{[i]}, \tag{2b}$$

for $i \in \mathcal{N}'$. For the sake of simplicity, without any loss of generality, we assume the catenary grid connected to the first carriage, and injecting the current $I_{\mathrm{DC}\ell}^{[0]}$. The dynamics of the injected current from the catenary is

$$\dot{I}_{\mathrm{DC}\ell}^{[0]} = \tfrac{1}{L_{\mathrm{DC}\ell}^{[0]}}\left(-R_{\mathrm{DC}\ell}^{[0]}I_{\mathrm{DC}\ell}^{[0]} + V_0 - V_{\mathrm{DC}}^{[1]}\right)\delta, \tag{3}$$

where V_0 is the catenary voltage at the DC-link, modelled as constant, while δ is a time-varying boolean parameter, where $\delta = 1$ if the catenary is connected to the train. Since the current $I_{\mathrm{DC}\ell}^{[0]}$ is null when the catenary is disconnected, this is bounded as

$$\underline{I}_{\mathrm{DC}\ell}^{[0]}\delta \leq I_{\mathrm{DC}\ell}^{[0]} \leq \bar{I}_{\mathrm{DC}\ell}^{[0]}\delta. \tag{4}$$

2.2 Batteries

The variables of interest for the battery model are the open-circuit voltage $E_{\mathrm{c}}^{[i]}$, the battery capacity $c_{\mathrm{c}}^{[i]}$, the internal resistance $R_{\mathrm{c}}^{[i]}$, the current $I_{\mathrm{c}}^{[i]}$, and the voltage $V_{\mathrm{c}}^{[i]}$. Considering the battery internal circuit, according to the following Kirchhoff's voltage law, it follows that

$$V_{\mathrm{c}}^{[i]} - E_{\mathrm{c}}^{[i]} = R_{\mathrm{c}}^{[i]}I_{\mathrm{c}}^{[i]}, \tag{5}$$

where the open-circuit voltage $E_{\mathrm{c}}^{[i]}$ is assumed constant. Neglecting the power losses inside the DC/DC-converter (typically very low due to their high efficiency), the power balance around the battery converter can be written as

$$V_{\mathrm{b}}^{[i]}I_{\mathrm{DCb}}^{[i]} = V_{\mathrm{c}}^{[i]}I_{\mathrm{c}}^{[i]}. \tag{6}$$

In fact, possible battery losses are captured by the presence of the internal resistance $R_{\mathrm{c}}^{[i]}$, as evident by combining (5) and (6) as follows

$$V_{\mathrm{b}}^{[i]}I_{\mathrm{DCb}}^{[i]} = E_{\mathrm{c}}^{[i]}I_{\mathrm{c}}^{[i]} + R_{\mathrm{c}}^{[i]}(I_{\mathrm{c}}^{[i]})^2. \tag{7}$$

The state of charge (SoC) of the battery is given by

$$\mathrm{SoC}^{[i]}(t) = \mathrm{SoC}^{[i]}(0) + E_{\mathrm{c}}^{[i]}\int_0^t \frac{I_{\mathrm{c}}^{[i]}(z)}{c_{\mathrm{c}}^{[i]}}\,\mathrm{d}z. \tag{8}$$

2.3 Drivetrain and auxiliary load AC-network

Fig. 2 shows in detail also the schematic single-line diagram of the drivetrain and auxiliary loads circuits, derived from (Buzzi et al., 2020). While the former is modelled as a current generator downstream of the impedance $R_{\mathrm{t}}^{[i]}L_{\mathrm{t}}^{[i]}$, the latter is connected in parallel to the generator, namely $I_{\mathrm{T}}^{[i]}$, and consists of the impedance $R_{\mathrm{a}}^{[i]}L_{\mathrm{a}}^{[i]}$ upstream of the VSC, and the filter $R^{[i]}L^{[i]}C^{[i]}$ downstream of the VSC, which is a pulse width modulation (PWM) converter transforming the DC signals to AC ones. The resistive-inductive component of filter $R^{[i]}L^{[i]}$ plays a role in extracting the fundamental frequency of the VSC output voltage, while the capacitor $C^{[i]}$ determines the output voltage of the ith load indicated with $v_C^{[i]}$, as well as the corresponding output current, namely $\imath^{[i]}$. Finally, the circuit comprises a ZI-load, i.e., nonlinear load with the parallel combination of constant impedance (Z) component, given by $R_{\mathrm{L}}^{[i]}$, and current (I) component, namely $\imath_{\mathrm{L}}^{[i]}$. Moreover, all the loads are connected in parallel through resistive-inductive lines with $R_\ell^{[i]}L_\ell^{[i]}$ impedance. Note that all the resistance and inductance values are scalar and equal for each phase.

Applying the Kirchhoff's voltage and current laws, in the so-called *abc*-frame, the corresponding model is

$$\frac{d\imath^{[i]}}{dt} = \frac{1}{L^{[i]}}\left(v^{[i]} - v_C^{[i]} - R^{[i]}\imath^{[i]}\right), \tag{9a}$$

$$\frac{dv_C^{[i]}}{dt} = \frac{1}{C^{[i]}}\left(\imath^{[i]} + \imath_\ell^{[i-1]} - \imath_\ell^{[i]} - \frac{v_C^{[i]}}{R_{\mathrm{L}}^{[i]}} - \imath_{\mathrm{L}}^{[i]}\right), \tag{9b}$$

for $i \in \mathcal{N}$, where $\imath^{[i]}, \imath_{\mathrm{L}}^{[i]}, v^{[i]}, v_C^{[i]}$ are 3×1 column vectors (one entry for each phase) representing the VSC output current, the load current, the VSC output voltage and the capacitor voltage, respectively. Note that, in (9), one has $\imath_\ell^{[0]} = 0$. Considering the electric lines of the auxiliary load circuit, the dynamics of the line current $\imath_\ell^{[i]}$ is

$$\frac{di_\ell^{[i]}}{dt} = \frac{1}{L_\ell^{[i]}}\left(v_C^{[i]} - v_C^{[i+1]} - R_\ell^{[i]} i_\ell^{[i]}\right), \tag{9c}$$

for $i \in \mathcal{N}'$.

In order to achieve a state model of system (9) in a suitable form for control design, each three-phase variable $s \in \left\{i^{[i]}, i_{\mathrm{L}}^{[i]}, i_\ell^{[i]}, v^{[i]}, v_C^{[i]}\right\}$ can be transferred to the synchronous rotating dq-frame by using the Clarke's and Park's transformations. The latter are given by

$$s_{\alpha\beta} = s_a \mathrm{e}^{j0} + s_b \mathrm{e}^{j\frac{2\pi}{3}} + s_c \mathrm{e}^{j\frac{4\pi}{3}}, \tag{10a}$$

$$S_{dq} = S_d + jS_q = s_{\alpha\beta}\mathrm{e}^{j\theta}, \tag{10b}$$

where $S \in \left\{I^{[i]}, I_{\mathrm{L}}^{[i]}, I_\ell^{[i]}, V^{[i]}, V_C^{[i]}\right\}$ are the dq variable and $\theta = \int_{t_0}^{t} \omega_0 \mathrm{d}z$ is the Park's transformation phase-angle related to the rated angular frequency $\omega_0 = 2\pi f_0$. Hence, the corresponding dq-frame model becomes

$$\dot{I}_d^{[i]} = \frac{1}{L^{[i]}}\left(V_d^{[i]} - V_{Cd}^{[i]} - R^{[i]} I_d^{[i]}\right) + \omega_0 I_q^{[i]}, \tag{11a}$$

$$\dot{I}_q^{[i]} = \frac{1}{L^{[i]}}\left(V_q^{[i]} - V_{Cq}^{[i]} - R^{[i]} I_q^{[i]}\right) - \omega_0 I_d^{[i]}, \tag{11b}$$

$i \in \mathcal{N}$, for the VSC filter equation (9a),

$$\dot{V}_{Cd}^{[i]} = \frac{1}{C^{[i]}}\left(I_d^{[i]} + I_{\ell d}^{[i-1]} - I_{\ell d}^{[i]} - \frac{V_{Cd}^{[i]}}{R_{\mathrm{L}}^{[i]}} - I_{\mathrm{L}d}^{[i]}\right) + \omega_0 V_{Cq}^{[i]}, \tag{11c}$$

$$\dot{V}_{Cq}^{[i]} = \frac{1}{C^{[i]}}\left(I_q^{[i]} + I_{\ell q}^{[i-1]} - I_{\ell q}^{[i]} - \frac{V_{Cq}^{[i]}}{R_{\mathrm{L}}^{[i]}} - I_{\mathrm{L}q}^{[i]}\right) - \omega_0 V_{Cd}^{[i]}, \tag{11d}$$

$i \in \mathcal{N}$, for current node balance (9b), while

$$\dot{I}_{\ell d}^{[i]} = \frac{1}{L_\ell^{[i]}}\left(V_{Cd}^{[i]} - V_{Cd}^{[i+1]} - R_\ell^{[i]} I_{\ell d}^{[i]}\right) + \omega_0 I_{\ell q}^{[i]} \tag{11e}$$

$$\dot{I}_{\ell q}^{[i]} = \frac{1}{L_\ell^{[i]}}\left(V_{Cq}^{[i]} - V_{Cq}^{[i+1]} - R_\ell^{[i]} I_{\ell q}^{[i]}\right) - \omega_0 I_{\ell d}^{[i]} \tag{11f}$$

$i \in \mathcal{N}'$, for the line equation (9c). Finally, assuming again to neglect the power losses inside the VSC, the power balance around the converter is

$$V_{\mathrm{a}}^{[i]} I_{\mathrm{DCa}}^{[i]} = \frac{3}{2}\left(V_d^{[i]} I_d^{[i]} + V_q^{[i]} I_q^{[i]}\right). \tag{12}$$

3. THE PROPOSED MPC-BASED ENERGY MANAGEMENT SYSTEM

For the sake of compactness, let us define the following vectors including the variables previously defined, omitting also here the time dependence for the sake of clarity,

$$x^{[i]} = [I_{\mathrm{DCb}}^{[i]}, I_{\mathrm{DCa}}^{[i]}, I_{\mathrm{DCt}}^{[i]}, I_{\mathrm{DC}\ell}^{[i]}, I_d^{[i]}, I_q^{[i]}, V_{Cd}^{[i]}, V_{Cq}^{[i]}, I_{\ell d}^{[i]}, I_{\ell q}^{[i]}]',$$

$$u^{[i]} = [V_{\mathrm{b}}^{[i]}, V_{\mathrm{a}}^{[i]}, V_{\mathrm{t}}^{[i]}, V_{\mathrm{DC}}^{[i]}, V_{\mathrm{c}}^{[i]}, I_{\mathrm{c}}^{[i]}, V_d^{[i]}, V_q^{[i]}]',$$

$$d^{[i]} = [V_0,\ I_{\mathrm{T}}^{[i]}, I_{\mathrm{L}d}^{[i]}, I_{\mathrm{L}q}^{[i]}]'.$$

The dynamical equations (1), (2a), (3), (11) are written as

$$\dot{x}^{[i]} = f(x^{[i]}, u^{[i]}, d^{[i]}), \tag{13}$$

where $f(\cdot)$ is a properly defined vector function. Moreover, equations (2b),(5),(6),(12), are compacted as

$$g(x^{[i]}, u^{[i]}, d^{[i]}) = 0\,, \tag{14}$$

where $g(\cdot)$ is a properly defined vector function. Moreover, all train electric variables must be constrained within their physical limits, implying that

$$\underline{x}^{[i]} \le x^{[i]} \le \bar{x}^{[i]}, \tag{15a}$$

$$\underline{u}^{[i]} \le u^{[i]} \le \bar{u}^{[i]}. \tag{15b}$$

Since our goal is to design an MPC-based management system for the electric devices of the train, we assume that the proposed approach plays the role of a high-level controller which generates voltage or current references to low-level regulators. Note that the design of the stabilizing low-level current and voltage regulators is beyond the scope of this paper, and we refer to (Nahata et al., 2021; Incremona et al., 2017) for possible solutions.

Having in mind a high-level controller, we consider the MPC running at slower rate, and, given the train circuit model, this is included as static in the MPC problem formulation, being electric transients typically much faster than the MPC sampling time $\tau_{\mathrm{s}} \in \mathbb{R}$ (see La Bella et al. (2018)). Therefore, (13) is included in the MPC formulation at its equilibrium, implying that

$$f(x^{[i]}, u^{[i]}, d^{[i]}) = 0. \tag{16}$$

We are now in a position to introduce the proposed MPC system. This is designed to be solved in discrete time domain at each generic time instant $t = k\tau_{\mathrm{s}} \in \mathbb{R}$, where $k \in \mathbb{N}_{\ge 0}$. The prediction horizon is defined as $\mathcal{T}_k \coloneqq \{k, \dots, k+N-1\}$, with the integer $N \ge 1$ be the horizon length. Also the dynamics of the SoC in batteries must be defined in discrete-time, so that by applying the forward Euler method to (8) one has

$$\mathrm{SoC}^{[i]}(k+1) \;=\; \mathrm{SoC}^{[i]}(k) \;+\; \frac{E_{\mathrm{c}}^{[i]} I_{\mathrm{c}}^{[i]}(k)}{c_{\mathrm{c}}^{[i]}}\,\tau_{\mathrm{s}}\,. \tag{17}$$

The battery $\mathrm{SoC}^{[i]}$ is bounded as follows

$$\underline{\mathrm{SoC}}^{[i]} \le \mathrm{SoC}^{[i]}(k) \le \overline{\mathrm{SoC}}^{[i]}, \tag{18}$$

where $0 \le \underline{\mathrm{SoC}}^{[i]} < \overline{\mathrm{SoC}}^{[i]} \le 1$.

The MPC problem for battery trains should be designed to accomplish the following objectives, agreed with the industrial partner Alstom rail transport:

(1) Batteries must be normally operated with a SoC higher than a pre-defined threshold $\mathrm{SoC}^{\mathrm{th}}$ (e.g., 50%) so as to ensure that a sufficient charge is available in case of catenary-free sections of the track. This is included with a soft constraint, i.e.,

$$\mathrm{SoC}^{[i]}(k) \;\ge\; \mathrm{SoC}^{\mathrm{th}} - \Delta s^{[i]}(k)\,, \tag{19}$$

where $\Delta s^{[i]} \ge 0$ is a slack variable that will be highly penalized in the MPC cost function.

(2) When the train brakes, the current regenerated from the traction (i.e., when $I_{\mathrm{T}}^{[i]} < 0$) must be charged in the batteries and not injected back in the catenary, provided that battery limits are not exceeded. This is formulated through the following soft constraint

$$I_{\mathrm{DC}\ell}^{[0]}(k) \ge -\Delta I_{\mathrm{cat}}(k)\,, \tag{20}$$

where $\Delta I_{\mathrm{cat}} \ge 0$ is a slack variable highly penalized in the MPC cost function.

(3) The train electric circuit must be operated at maximum efficiency, minimizing power losses while transferring energy from/to batteries to/from carriages. Defining the vector of all train currents as

$$\mathcal{I}^{[i]} = [I^{[i]}_{\mathrm{DCb}},\, I^{[i]}_{\mathrm{DCa}},\, I^{[i]}_{\mathrm{DCt}},\, I^{[i]}_{\mathrm{DC}\ell},\, I^{[i]}_{\mathrm{c}},\, I^{[i]}_{d},\, I^{[i]}_{q}, I^{[i]}_{\ell d},\, I^{[i]}_{\ell q}]',$$

and the diagonal matrix $\mathcal{R}^{[i]}$ including all resistances

$$\mathcal{R}^{[i]} = \mathrm{diag}\{R^{[i]}_{b}, R^{[i]}_{a}, R^{[i]}_{t}, R^{[i]}_{\mathrm{DC}\ell}, R^{[i]}_{c}, R^{[i]}, R^{[i]}, R^{[i]}_{\ell}, R^{[i]}_{\ell}\},$$

the total active power loss in the train circuit is

$$P_{\mathrm{loss}}(k) = \sum_{i=1}^{n} \mathcal{I}^{[i]}(k)'\, \mathcal{R}^{[i]}\, \mathcal{I}^{[i]}(k)\,. \qquad (21)$$

Thus, the following MPC optimization problem is solved at each $t = k\tau_{\mathrm{s}}$, i.e.,

$$\min_{u(\cdot)} \sum_{h=k}^{k+N-1} P_{\mathrm{loss}}(h) + \gamma_{\mathrm{cat}} \Delta I_{\mathrm{cat}}(h)^2 + \gamma_s \sum_{i=1}^{n} \Delta s^{[i]}(h)^2,$$

subject to (4), (14)–(21), $\forall h \in \mathcal{T}_k$,

where $\gamma_{\mathrm{cat}} > 0$ and $\gamma_s > 0$ are properly defined weights.

4. CASE STUDY

In this section, the proposal is assessed in simulation relying on real data provided by Alstom rail transport.

4.1 Settings

The simulation scenario consists of a regional train having $n = 4$ carriages and it moves over a track with two stops. The electric equipment of the train is structured as follows. The first and the fourth carriages (i.e., $i = 1$ and $i = 4$) are equipped with both batteries and traction motors, while the other two (i.e., $i = 2$ and $i = 3$) are "buggy" carriages. Then, all the carriages present a circuit for auxiliary loads. Moreover, during the journey, the train crosses a catenary-free section of the track in the interval $t \in [80, 140]$ min. In the following figures, the time instants where the catenary grid is absent are highlighted in a shadow window. Making reference to the single-line electric diagram, all the parameters values, equal for each carriage, are reported in Table 2. The motor current required by the train or regenerated during braking is reported in Fig. 3 (left) for carriage 1 (the current profile for carriage 4 is the same), together with the direct current absorbed by the auxiliary loads (right).

As for the proposed MPC, the sampling time is $\tau_{\mathrm{s}} = 60\,\mathrm{s}$ and the horizon is $N = 30$, while the cost function weights are $\gamma_{\mathrm{cat}} = 1 \times 10^4$ and $\gamma_s = 1 \times 10^5$. The desired threshold $\mathrm{SoC}^{\mathrm{th}}$ is set equal to 0.6. It is worth noting that the prediction of disturbances is assumed to be known at the MPC level, e.g., derived from historical data of past train travels in the same track.

4.2 Results

Fig. 4 illustrates the SoC profiles for the two batteries in carriages 1 and 4. As expected, starting from an initial SoC equal to 0.8, both SoCs decrease but with different

Table 2. Electric parameters.

V_0	650	V
E_{c}	800	V
ω_0	$2\pi 50$	$\mathrm{rad\,s^{-1}}$
c_{c}	165	kW h
R_{L}	1×10^2	Ω
$R_{\mathrm{b}}, R_{\mathrm{a}}, R_{\mathrm{t}}, R, R_{\mathrm{c}}, R_{\ell}$	1×10^{-3}	Ω
$R_{\mathrm{DC}\ell}$	4×10^{-3}	Ω
$L_{\mathrm{DC}\ell}$	20×10^{-6}	H
L_{ℓ}	1×10^{-3}	H
L	1×10^{-6}	H
C	1×10^{-6}	F

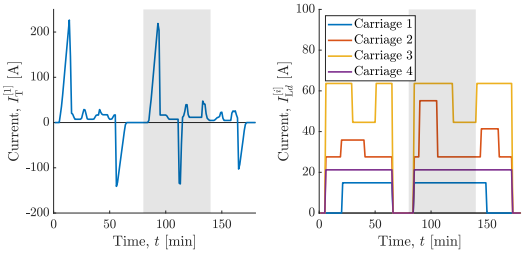

Fig. 3. Profiles of traction/braking current $I^{[1]}_{\mathrm{T}}$ (left), and of direct load current $I^{[i]}_{\mathrm{Ld}}, i = 1, 2, 3, 4$ (right).

rate by virtue of the minimization of losses operated by the MPC. Indeed, since the auxiliary load of carriage 3 is higher than the others, battery 4, which is the closer one, is more involved in supplying it. Then, around the time instant 50 min, both batteries are charged due to the prediction operated by the MPC which foresees the presence of a catenary-free section of the track. Therefore, in the interval $t \in [80, 140]$ min the two batteries discharge again to supply both traction and auxiliary loads, and when the train connects again with the catenary, they start to charge up to the desired threshold equal to 0.6.

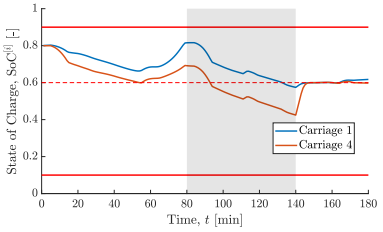

Fig. 4. SoC profiles for the batteries on carriages 1 and 4.

The time evolution of the battery currents $I^{[i]}_{\mathrm{DCb}}$, $i = 1, 4$ is reported in Fig. 5. It is evident from the beginning that in order to minimize losses over the lines, the MPC makes the batteries supply part of the traction and load. Then, coherently to the SoC profiles, when the train brakes (e.g., in $t \in [50, 60]$ min in Fig. 3) and regenerative energy is provided to the lines, the batteries start to charge, thus avoiding to transfer the regenerated energy to the catenary.

The currents flowing through DC lines interconnecting all the carriages are reported in Fig. 6, where it can be noticed that the MPC decides to absorb higher amount of current from the catenary either to charge batteries or, when needed, to supply traction peaks.

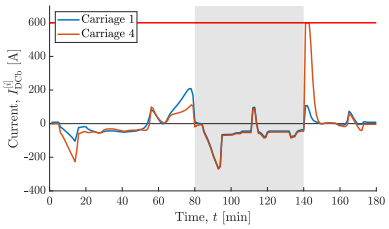

Fig. 5. Profiles of battery current $I^{[i]}_{\mathrm{DCb}}$, $i = 1, 4$.

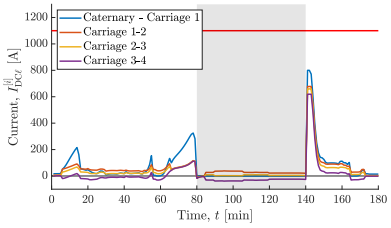

Fig. 6. Profiles of DC line currents $I^{[i]}_{\mathrm{DC}\ell}, i = 1, 2, 3, 4$ between carriages.

Finally, the total energy losses for the simulated scenario amount to 0.78 kW h. Furthermore, the MPC problem has been solved in Matlab, using IPOPT optimizer with an average computational time equal to 2 s.

The performances of the designed MPC are compared with an heuristic control strategy for managing trains equipped with batteries. The latter implies the following rules:

- Batteries are activated when the catenary is not present. Moreover, in this case the current absorption by auxiliary loads and traction motors is equally shared among batteries, according to standard *current sharing* strategies.
- Capacitor voltages in the auxiliary circuit are all constant and equal to the nominal reference 325 V, see, e.g., (Buzzi et al., 2020).
- Battery voltages at the DC circuit are all constant and equal to the nominal reference 650 V.
- If the SoC of batteries goes below the threshold $\mathrm{SoC}^{\mathrm{th}}$ due to a catenary-free track, batteries are charged up to 0.8 as soon as catenary is reconnected.

Applying the heuristic control strategy to the same scenario, the overall energy losses are 1.58 kW h, implying that the proposal enables to achieve a 50.7% power saving.

5. CONCLUSIONS

In this article, we have presented an MPC approach to solve the energy-management problem for a train, whose most carriages are equipped with parallel-connected auxiliary loads, and some of them also with traction motors and batteries. We have discussed the cost function design on the basis of efficient energy management, and we have provided a solution to deal with even a large amount of optimization variables in real time. The proposal allows also to efficiently govern the batteries in the case of partial catenary-free scenarios, thus paving the way for several extensions, such as fully catenary-free rails, hydrogen fuel-cells trains and multi-trains networks.

REFERENCES

Al-Ezee, H., Tennakoon, S.B., Taylor, I., and Scheidecker, D. (2015). Aspects of catenary free operation of DC traction systems. In *50th International Universities Power Engineering Conf.*, 1–5. Stoke-on-Trent, UK.

Albrecht, A., Howlett, P., Pudney, P., Vu, X., and Zhou, P. (2016). The key principles of optimal train control–part 1: Formulation of the model, strategies of optimal type, evolutionary lines, location of optimal switching points. *Transportation Research Part B: Methodological*, 94, 482–508.

Alstom (2016). Alstom unveils Coradia iLint hydrogen fuel cell powered train for european regional market. *Fuel Cells Bulletin*, 2016(9), 1.

Becker, F. and Dämmig, A. (2016). Catenary free operation of light rail vehicles–topology and operational concept. In *18th European Conference on Power Electronics and Applications*, 1–10. Karlsruhe, Germany.

Buzzi, A.C., Incremona, G.P., Colaneri, P., Dolcini, A., and Colombo, A. (2020). Sliding mode based droop control strategies for parallel-connected inverters in railway vehicles. In *European Control Conference*, 1891–1896. St. Petersburg, Russia.

Campillo, J., Dahlquist, E., Danilov, D.L., Ghaviha, N., Notten, P.H.L., and Zimmerman, N. (2017). *Battery Technologies for Transportation Applications*, 151–206. Springer International Publishing, Cham.

Farooqi, H. (2019). *Design of Collaborative Eco-Drive control Algorithms for Train Networks*. Ph.D. thesis, Politecnico di Milano.

Farooqi, H., Incremona, G.P., and Colaneri, P. (2019). Railway collaborative ecodrive via dissension based switching nonlinear model predictive control. *European Journal of Control*, 50, 153–160.

Howlett, P. (2000). The optimal control of a train. *Annals of Operations Research*, 98, 65–87.

Incremona, G.P., Cucuzzella, M., Magni, L., and Ferrara, A. (2017). MPC with sliding mode control for the energy management system of microgrids. In *20th IFAC World Congress*, 7397–7402. Tolosa, France.

Kim, J., Guerrero, J.M., Rodriguez, P., Teodorescu, R., and Nam, K. (2011). Mode adaptive droop control with virtual output impedances for an inverter-based flexible ac microgrid. *IEEE Transactions on Power Electronics*, 26(3), 689–701.

La Bella, A., Negri, S., Scattolini, R., and Tironi, E. (2018). A two-layer control architecture for islanded ac microgrids with storage devices. In *2018 IEEE conference on control technology and applications (CCTA)*, 1421–1426. IEEE.

Li, M., Gui, Y., Jin, Z., Guan, Y., and Guerrero, J.M. (2018). A synchronous-reference-frame I-V droop control method for parallel-connected inverters. In *International Power Electronics Conference*, 2668–2672. Niigata, Japan.

Nahata, P., Bella, A.L., Scattolini, R., and Ferrari-Trecate, G. (2021). Hierarchical control in islanded dc microgrids with flexible structures. *IEEE Transactions on Control Systems Technology*, 29(6), 2379–2392.

Scheepmaker, G.M., Goverde, R.M., and Kroon, L.G. (2017). Review of energy-efficient train control and timetabling. *European Journal of Operational Research*, 257(2), 355–376.